JOURNAL OF PROPULSION AND POWER
Vol. 18, No. 2, March–April 2002

Combustion Air Jet Influence on Primary Zone Characteristics for Gas-Turbine Combustors

S. Gogineni*
Systems Research Laboratories, Dayton, Ohio 45440-3696
D. Shouse,† C. Frayne,‡ and J. Stutrud†
U.S. Air Force Research Laboratory, Wright–Patterson Air Force Base, Ohio 45433-7103
and
G. Sturgess§
Pratt & Whitney, East Hartford, Connecticut 06108

Results are presented of emissions and lean blowout measurements in a generic combustor primary zone of an aircraft gas-turbine engine for the effects of opposed, circular combustion air jets of a range of sizes, positioned half a dome height downstream from the dome. The primary zone was operated at simulated engine high-power conditions and representative dome and liner pressure drops. Most of the NO_x is generated in the jets. Although an optimum jet size is identified, the lowest overall emissions resulted from a no-combustion air-jet configuration; air jets are necessary, however, to confer lean blowout stability and short flame length.

Nomenclature

F	=	$10^{0.00143T}/3.72$, temperature correction factor (to 400 K)
H_d	=	combustor dome height
K_f	=	flow criterion
$\dot{m}$	=	mass flow rate through combustor, lbm/s
n	=	apparent reaction order
P	=	combustor pressure, atm
$T_{\dot{m}}$	=	temperature of inlet air, K
V	=	combustor volume, ft^3
Δp	=	pressure drop across combustor
ΔT	=	temperature rise across combustor
$\rho_{\dot{m}}$	=	density of air under combustor inlet conditions
ϕ	=	equivalence ratio

Introduction

DURING development of combustors for industrial and aircraft gas-turbine engines, the issues of adequate lean blowout (LBO) margin and low exhaust emissions are both important aspects in the design process. It is increasingly more difficult to ensure that designs have adequate stability margins concurrently with low emissions and high temperature rise. Achievement of flame stability over wide ranges of engine operating conditions is a function of the primary zone of the combustor; the flame structures established in the primary zone will also control the exhaust emissions. Many aircraft engine combustors use transverse air jets introduced through the liners to provide a nominal termination of the primary zone. These air jets also supply some part of the total air necessary for complete combustion of the fuel. Almost nothing exists in the open literature concerning the interactions of the jet and dome flows in determining emissions or lean blowout stability.

Program Objectives

The overall intent of the study was to understand the detailed behavior of the major flame-holding region (the primary zone) of a generic modern combustor for aircraft gas-turbine engines.

The comprehensive objective was to determine the major flowfield features of a representative primary zone and to understand how they control lean stability together with gaseous emissions generation. It was intended to establish how these specifics are affected by liner and dome pressure drops, and combustion air port positions, shapes, sizes, and arrangements.

Combustor Configuration

The experimental combustor used in this study was modified from one used in an earlier program[1] and was designated the PW 150 technology combustor.[2] The purpose of the combustor was to provide an approximate representation of the salient flame-holding features of a gas-turbine annular combustor in a simplified geometric configuration having high optical access. The combustor cross section, therefore, represented a compromise between the requirements of simplicity for modeling purposes and uncomplicated optical access for application of laser diagnostics. The cross section was square, but generous circular-arc fillets were provided in the corners to suppress vorticity generation that might result in spurious flame holding.

The PW 150 combustor for the present program (Fig. 1) contained a high-swirl (HS) airblast atomizing fuel injector[3] (modified for gaseous fuel operation) and its dome interfacing system. The combustor included uncooled solid metal top and bottom combustor liner plates that accommodated suitable arrays of combustion air jets. Typical flame structures are shown in Fig. 2 for 0.375-in.-(9.53-mm) diam plain circular jets positioned at half-dome height downstream and operating at an overall equivalence ratio of 1.2 with a liner pressure drop of 2.7%. One side combustor liner plate (at 90 deg to the liner plates containing the air jets) contained a fitting for a torch igniter and the other had a quartz window for visual access. The combustor length was 490 mm, and the combustor had a 153-mm hydraulic diameter. The combustor outlet was restricted by a 45% geometric blockage orifice plate[3] to provide representative backpressure of the remainder of a real combustor. The presence of the backpressure plate also prevented the recirculation of external air from downstream back into the combustor.

Received 29 August 1996; revision received 18 October 2001; accepted for publication 20 October 2001.

*Research Engineer, 2800 Indian Ripple Road; currently Senior Engineer, Innovative Scientific Solutions, Inc., 2766 Indian Ripple Road, Dayton, Ohio 45440-3638. Associate Fellow AIAA.
†Mechanical Engineer, Aero Propulsion and Power Directorate.
‡Electronic Engineer, Aero Propulsion and Power Directorate.
§Fellow; currently Corporate Vice-President, Innovative Scientific Solutions, Inc., 2766 Indian Ripple Road, Dayton, Ohio 45440-3638. Fellow AIAA.

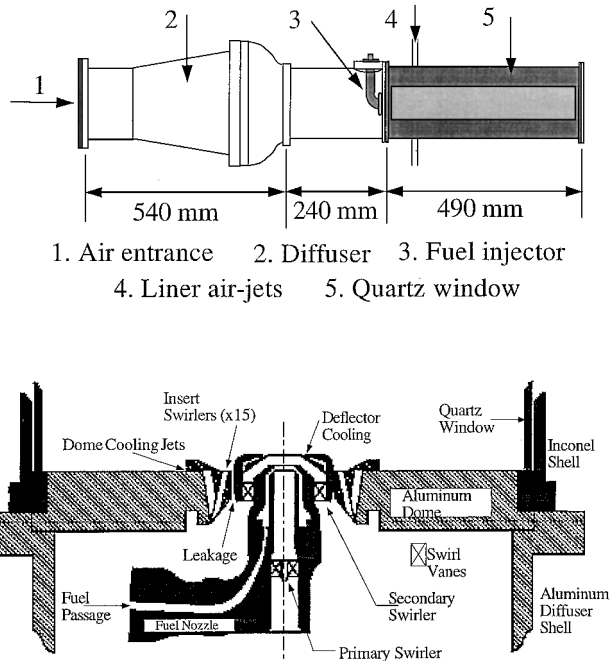

Fig. 1 Laboratory-scale gas-turbine combustor primary zone, showing fuel injector and dome configuration.

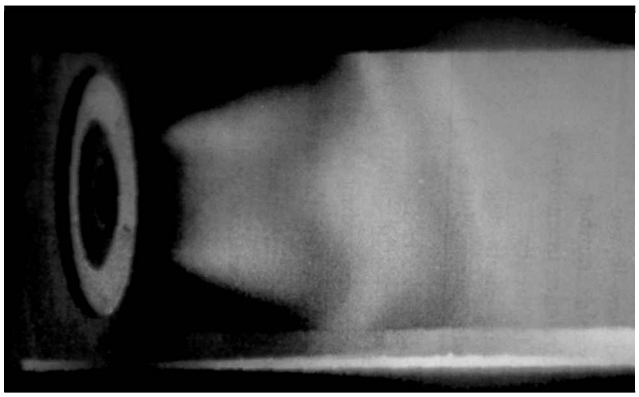

Fig. 2 Natural light flame photograph showing flame structure for the 0.375-in.- (9.53-mm) diam air jets at the half-dome height position.

In the configuration described, the modified combustor represented, in simplified form, the features of the dome and primary zone regions of a generic gas-turbine combustor.

Efficacy of PW 150 Combustor

The PW 150 combustor represented a "single-cup," planar segment of an annular combustor and simulated the primary zone only. It was operated at atmospheric pressure. Therefore, given these limitations it is necessary to justify its acceptability for the intended purpose.

A planar segment of any combustor sacrifices an important aspect of real annular combustors in that the cross-sectional flow areas above and below the combustor midplane surface are symmetrical, which they are not in reality as a result of liner curvatures. The biggest effects of this difference are seen in liner temperatures and the exit mean radial temperature profile, neither of which is of interest to the present program.

Having physical side walls (reflecting), the single-cup combustor has symmetry in lateral boundary conditions rather than periodicity in lateral boundary conditions as in a complete annular system. This means that significant interactions taking place between adjacent cups in a real annular combustor will not be present in the single-cup model combustor. This discrepancy could clearly exert some influence on the overall emissions. However, the general behavior of the individual cup module of an annular combustor that is made up of a circumferential arrangement of such modules should not be substantially changed. Therefore, the single-cup combustor does allow a useful study to be made of the general characteristics pertaining to individual module behavior.

Operation of a study at atmospheric pressure requires that there be no changes in combustor flow patterns between the study and the application operating at high pressures. Application of the laws of partial modeling[4] shows that the aerodynamic processes determining the combustor flow pattern are established by combustor geometry, air pressure drops across the combustor dome and liners, and Reynolds number; Mach numbers are sufficiently low that they exert no effects on flow pattern. Temperature changes caused by heat release from chemical reaction cause changes in velocity and velocity gradients at all points in the combustor, and these can result in some local effects of significance; but if the Reynolds number is high and Mach number is low, these might be neglected overall. Generally, the main features of flow pattern should not be affected. Overall fuel-to-air ratio exerts an effect through the influence of fuel momentum. This has little significance except near the fuel injector where the liquid spray is dense. Fortunately, airblast atomization of liquid fuel from high-flow-number fuel injectors, as used in most modern combustors, ameliorates even this local effect because the fuel has little momentum of its own and is dispersed across the combustor by the air motions. Gaseous propane was used as the fuel for these simulations. Given the fine atomization of liquid fuel achieved by airblast atomization together with the high droplet evaporation rates existing at high-power engine conditions, propane was considered as appropriate for the simulation.

These arguments produce the useful half-truth that, to first order, the flow pattern depends only on the combustor geometry and the air pressure drop across it. Following Spalding,[4] dimensional analysis leads to the flow criterion K_f, where

$$K_f = \frac{\dot{m}^2}{\Delta p \rho_{\dot{m}} D^4 g_0} \tag{1}$$

where the characteristic dimension D is taken as the combustor dome height H_d, and g_0 is Newton's constant if English units are used. The flow criterion should be a constant, as close to unity as possible, between the model combustor and the application. Equation (1) forms the basis for the well-known water-analogy combustion tunnel,[5] through which many successful practical combustors have been developed in the past. The additional term $\Delta T/T_{\dot{m}}$ should also be accounted for.

At conditions representative of the tests, the PW 150 combustor was operated such that the ratio was

$$\frac{(K_f)_{\text{rig}}}{(K_f)_{\text{engine}}} = 1.22 \tag{2}$$

in comparison with a primary zone of a combustor in a 32-atmosphere engine at take-off power, and the ratio,

$$\frac{(\Delta T/T_{\dot{m}})_{\text{rig}}}{(\Delta T/T_{\dot{m}})_{\text{engine}}} = 1.67 \tag{3}$$

The value for the K_f ratio is quite acceptable; the value for the $\Delta T/T_m$ ratio is a little high. However, because $\Delta T/T_m$ only affects the local temperature and velocity gradients but not the overall size and shape of the flame structures, it can be concluded, therefore, that the PW 150 combustor can reproduce reasonably well and, to an acceptable degree, the flow patterns of an engine combustor.

Description of the Rig

The rig was mounted horizontally in a test cell of Wright Laboratory, Wright–Patterson Air Force Base, Ohio. Compressor air after being dried to very low dew points was supplied to the dome region of the combustor by a flow conditioner, passing first through a pressure regulator then through an orifice plate for flow measurement. The flow was controlled with a Fischer controller and valve.

The dome air was then passed through a 48-kW electric heater that utilizes a cascade control system to control the delivered air temperature to the rig. This particular heater could deliver 20 lb/min (9.07 kg/min) of air at 500°F (533 K).

A separate air supply and control system was incorporated to deliver air to the liners. The air was supplied by a 2200 psi bottled air trailer with the flow controlled by pressure and with sonic venturis for flow measurement; it was also dried to very low dew points. The air was then passed through a 15-kW electric heater before the air line was split to deliver air to the top and bottom liner jet bosses. A thermocouple located in the liner jet boss provided temperature feedback to the heater controller. This heater could deliver 5 lb/min (9.27 kg/min) of air at 500°F (533 K). Pressure transducers connected to static-pressure taps located in the dome and liner jet plenum provided a measure of the pressure drops across the dome and liners.

Gaseous propane was supplied from bottles that were ganged together. The propane was metered via turbine flow meters with the flow controlled by Fisher controllers and Badger research valves. The propane was filtered before being delivered to the rig. The fuel-air mixture in the combustor was ignited by a propane torch inserted through a port located in the side wall of the combustor in the near-dome region. The torch was withdrawn, and a blanking plug was inserted into the igniter port following a successful light. Cooling water and glycol for the emissions probe were pumped from a reservoir through the probe where a thermocouple monitored the exiting fluid from the probe. Before returning to the reservoir, the heated glycol was run through a heat exchanger to reduce its temperature.

Range of Experimental Variables

The geometric arrangement of the combustor for this study consisted of the airblast atomizing fuel injector (modified for operation on gaseous propane) mounted with its insert swirler and cooled dome heat shield in the combustor dome (Fig. 1b) and an associated pair of circular combustion air ports contained in the upper and lower walls of the combustor; the air ports were inline with the injector centerline. Although the pair of air ports could be situated 1.0, 0.75, and 0.5 dome heights (H_d) downstream from the dome, only data for the $H_d/2$ position are presently given. Air port diameters were 0.75, 0.5, 0.375, and 0.25 in. (19.05, 12.7, 9.53 and 6.35 mm, respectively), and the equivalent geometric area of the 0.5-in.-diam port in the form of four individual jets of 0.25 in. diam on a pitch circle of 0.575 in. (14.6 mm) diam. Only data for SJ ports are presently given.

The fuel injector was designated as the HS injector, and its design features were representative of current airblast atomizer technology. It had a nominal swirl number (based on vane angles and mass weighted for the swirler flow splits) of 1.41. The total air passage effective area was 0.176 in. (113.55 mm^2), with an outer to inner passage flow split of 2.8. The outer swirler vane angle was 55 deg, and the inner swirler vane angle was 70 deg. The inner passage swirl number was 1.91. The insert swirlers were angled 12.5 deg into the injector centerline, and the swirl angle was zero in this instance. The purpose of the insert swirlers is described in Sturgess et al.[3,6] Dome cooling air was introduced with, but separated from, the insert swirler air and was turned to flow radially outward along the dome surface by a circular deflector plate. The total effective airflow area of the dome excluding the fuel injector was 0.16 in^2 (103.23 mm^2).

The pressure drop across the dome was held fixed at a nominal 4.3% to represent the typical engine experience. To assess its importance, the pressure drop across the air ports was initially varied over the range of 1–5% of the upstream pressure. For the 0.50-in.-(12.7-mm) diam jet, the pressure drop range was extended to as high as 12% in order to explore the effects of jet overpenetration and high turbulence. The dome was also run alone (0% jet pressure drop) to assess the contribution to the total emissions of the injector separate from those of the closely coupled combustion air jets. Pressure drop across a combustor is in practice not a free variable but is set by engine performance considerations. Generally, the allowable pressure drop across a dome is a little higher than that across liners because of the recovery of some dynamic head from the compressor. For much of the work to be presented, the dome pressure drop was held fixed at a nominal value of 4.3% of the upstream pressure, and the liner pressure drop was 3.0%. These values are representative of typical engine conditions. Under these conditions all of the transverse jets with different initial diameters penetrated to the combustor centerline. The inlet air temperatures for the separate dome and transverse jet supplies was a nominal 500°F (533 K). This value was chosen to help satisfy the simulation criteria and to ensure generation of sufficient NO_x without large burn up of CO, so as to permit easy detection of trends and effects in these two pollutants.

With fixed dome and liner pressure drops, for each air-port size, axial position, and pressure drop, the fuel flow rate was varied to cover a range of overall equivalence ratios such that the minimum in the CO curve and the maximum in the NO_x curve could be fully established. It was demonstrated that fuel momentum was not affecting the emissions results.

For the blowout data the air-port pressure drop with a given geometric configuration and inlet air temperature was set in the range of 1–5% at a given dome pressure drop. At each air-port pressure drop the fuel flow was incrementally reduced until a lean blowout occurred.

Description of the Emission Measurements

The emissions sampling probe was a water-cooled quick quench type. This single-point probe was constructed of stainless steel and had an inconel tip. Combustion exhaust was drawn into the probe through a 0.059-in.-(1.5-mm) diam orifice of a converging nozzle. The inside passage diverged to the inside diameter of the sampling tube, which was 0.25 in.-(6.35-mm) diam stainless-steel tubing with a 0.180 in. (4.57 mm) inside diameter. The diverging passage in conjunction with the low pressure inside the probe created a short supersonic expansion, which reduced the temperature of the gas stream. This, combined with the water cooling, effectively quenched the combustion reactions inside the probe. The probe contained a 3-in.-(76.2-mm) diam 90-deg bend and was mounted on a mechanical traversing stand. Figure 3 shows a detail of the emissions probe sampling tip.

The sample transfer system consisted of the sampling probe and heated transfer lines. The probe was connected to $\frac{1}{4}$-in.-(6.35-mm) stainless-steel tubing that was electrically heated and enclosed in an

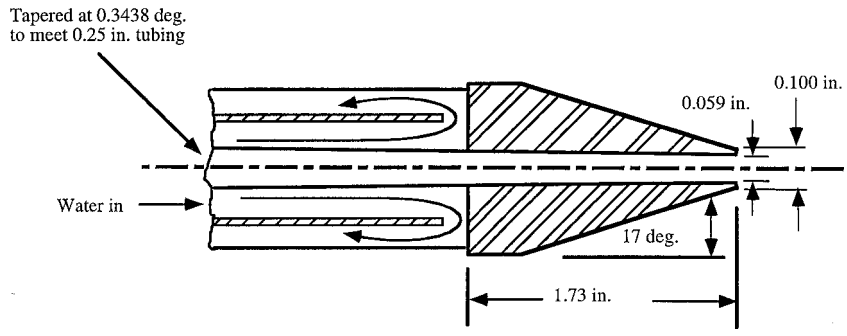

Fig. 3 Sampling tip of the emissions probe.

insulated outer cover. The line was maintained at 320°F (433 K) to prevent condensation of the sample. The line passed from the test cell into the control room and entered an oven, also maintained at 320°F (433 K), where the sample stream was passed through two particulate filters and entered a bellows pump that provided the driving force for the sample flow. The line was then split into two sections, one leading directly to a Beckman Model 402 total hydrocarbon analyzer and the main sample stream leading into a second oven where the line was tapped three more times for delivery to a Beckman Model 955 NO_x analyzer, a Beckman Model 864 CO_2 analyzer, and a Beckman Model 865 CO analyzer, respectively. The sample stream passing into the NO_x analyzer was measured wet. This oven and the lines leading from it were maintained at 160°F (344 K), which is just above the dew point of the exhaust emissions. The sample streams leading to the CO and CO_2 analyzers were first passed through a dryer, where the water content in the sample was extracted through a semipermeable membrane. A hygrometer measured the dew point at the dryer outlet; this temperature was necessary for correcting the dry concentrations back to wet concentrations when making the emissions calculations. The procedures for measuring wet concentrations of hydrocarbons and NO_x emissions and dry concentrations of CO and CO_2 emissions and for controlling the temperatures of the lines are in accordance with the sampling technique and measurement of these emissions as set forth in the Aerospace Recommended Practice, ARP 1256A, and Appendix 3 of International Civil Aviation Organization (ICAO) Annex 16, Volume 2. Although oxygen measurements were not included in any of the emissions calculations, a Beckman Model 755 oxygen analyzer was used to sample the stack exhaust, which contained the accumulated exhaust passed through each of the analyzers, plus any bypassed sample exhaust. NO_x was corrected to a humidity of 0.0063 lbm water per lbm air (0.00286 kg/kg).

In practice, span gases were used to calibrate the emissions analyzers at the ranges of interest. The CO and CO_2 analyzers are nondispersive infrared instruments, and nonlinear calibration curves are used for their calibration over a wide range of span gases. The other analyzers are linear instruments that require a single range calibration. Before each run, the calibrations were performed to less than 3% error. The accuracy of the calibrations was verified both during and after the test runs.

The emissions measurement system was interfaced to a Sun Microsystems computer and data acquisition system that converted analyzer output voltages to concentration values. The emissions calculations made conformed to the methods contained in Aerospace Information Report (AIR) 1533 and Appendix 3 of ICAO Annex 16, Volume 2.

During sampling, an equilibrium test condition was achieved when the analyzers had stabilized; for further accuracy oxygen stability ensured that the sampling system was saturated and an equilibrium condition existed. Further, comparison of the metered fuel-to-air ratio to the measured exhaust fuel-to-air ratio formed an effective representation of the carbon balance between fuel reactants and exhaust products. The agreements were always better than 10% for metered equivalence ratios of unity and less.

For each test condition it was first determined that the emission indices of NO_x (as NO_2), of CO, and of THC (as CH_4) ($EINO_x$, EICO, and EITHC in grams/kilogram of fuel burned) obtained by placing the probe at the center of the test section were the same as those measured by means of an area weighted average procedure. The emission measurements were obtained by traversing the probe both horizontally and vertically through the center of the measurement plane. The measurement plane was 14 in. (355.6 mm) downstream from the dome. Because the emissions probe was introduced into the combustor through the exit orifice plate of 45% blockage, the radial extent of these traverses was determined by this orifice plate. The extent of the radial profile traverses was ±1.75 in. (±44 mm) from the combustor centerline. The area weighted average procedure involved applying a curve fit to the emission measurements obtained in each direction and dividing the area of the combustor exit measurement plane into 11 concentric circles and into 21 sections. The interpolated points were chosen such that each point

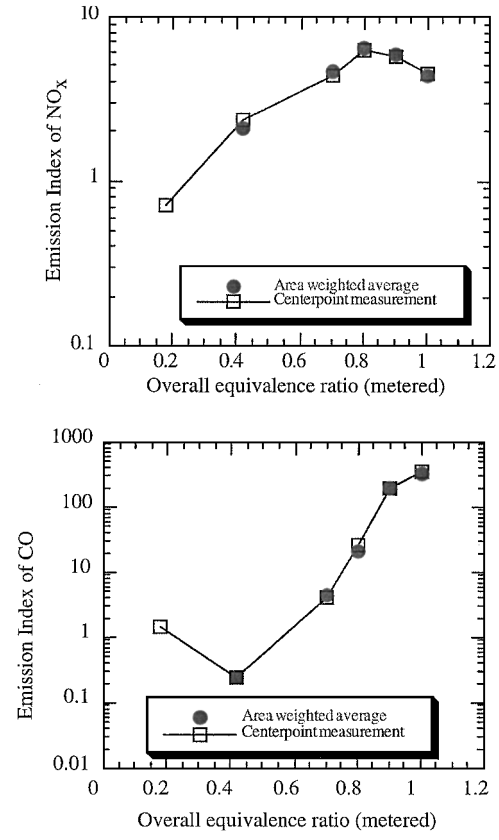

Fig. 4 Example of comparison of area weighted and centerpoint emissions measurements.

represents an equal area of the exit plane. These points were used to find the emission indices from the curve-fitting equation both in the horizontal and vertical directions. An area weighted average was then obtained from the average of these interpolated values. These weighted average emission measurements were compared with the centerpoint measurements, and a typical comparison for $EINO_x$ and EICO is shown in Fig. 4.

The figure indicates that well-mixed conditions occurred at the probe location, and the errors involved were within ±10%. The measurement station of 14 in. (355.6 mm) downstream from the dome was chosen to allow the complex flowfields from the combustion air jet interactions to mix out so that relatively flat emissions profiles were obtained. Such flat profiles, in conjunction with the area-weighting check procedure, allowed single-point measurements to represent the various emissions fields adequately. Of course, chemical reactions could continue beyond the jet-interaction plane before the measurement plane was reached. Check calculations were made, and these showed that CO levels continued to fall from the jet plane to the measurement station but were still reasonably high and that NO_x levels changed very little. The area weighted averaging analysis was performed at each and every test condition and was observed to exhibit the same trends as shown in Fig. 4. Based on this analysis, it was decided to present the emission measurements obtained by placing the probe at the central location of the measurement station in the present investigation.

Effects of Jet Pressure Drop

Figure 5 gives an example of the effect on emission indices of pressure drop across the air ports for the 0.5-in. (12.7-mm) jets as the overall metered equivalence ratio was varied. The transverse air jets were at the $H_d/2$ position, and the fixed dome pressure drop was 4.3%. Minima for carbon monoxide and unburned hydrocarbons are evident at overall equivalence ratios of around 0.42 and 0.7, respectively, and NO_x shows a maximum at an overall equivalence ratio around 0.9. Increasing jet pressure drop increases the peak NO_x significantly, from around 3.4 g/kg at zero pressure drop (dome

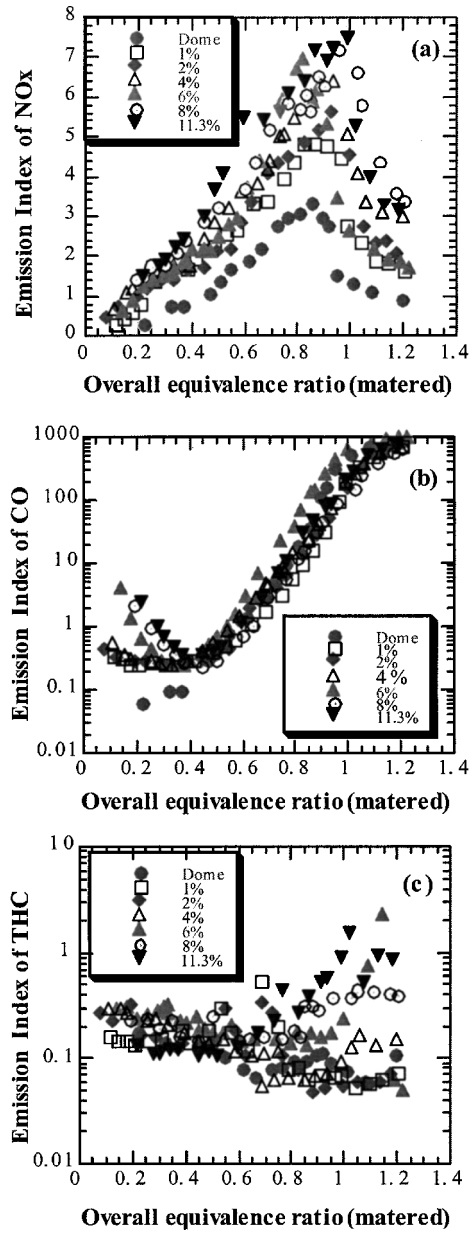

Fig. 5 Effect of liner pressure drop on emission for the 0.50-in. (12.7-mm) opposed air jets at the half-dome height position.

alone) to about 7.5 g/kg at 11.3% pressure drop. When the air jets are present, there is little effect of jet pressure drop on the minimum CO; however, the dome-alone data indicate that a CO minimum has not been reached for overall equivalence ratios down to about 0.2. At all other equivalence ratios the highest CO results from the highest pressure drop. The highest pressure drop also results in the highest emission indices of unburned hydrocarbons over the entire range of overall equivalence ratios. Again, there is no systematic dependence of unburned hydrocarbons on jet pressure drop. The low emissions performance of the dome alone (no transverse air jets) is noteworthy. With the low levels of CO and THC emission indices recorded, the combustion efficiency for all jet pressure drops was about 99.99% up to an overall equivalence ratio of about 0.8 and then decreased for higher equivalence ratios.

Visible in the flame structures seen in Fig. 2 is an intense central flame at the confluence of the opposed air jets that projects upstream slightly into the central region of the conical shear-layer flame from the fuel injector. The size of the central flame increased with increasing pressure drop. Computational fluid dynamics (CFD) analysis of a similar combustor and injector configuration[7] revealed that a football-like (ellipsoidal with the major axis in the same plane but normal to the combustor centerline) recirculation zone was situated immediately upstream of the confluence of the penetrating air jets. Flame appeared to be stabilized around this ball recirculation in a stoichiometric interface. Total emissions from the primary zone will depend on the number, size, and local conditions existing in the flame structures present. Obviously, operating conditions that increase the number or size of flame structures will result in changing emissions values.

Dome Characteristics

The combustor can be operated with zero-combustion air jets to obtain the characteristics of the dome alone. Figure 6 is a plot of the emission index of NO_x for the dome, as a function of metered equivalence ratio taken from Fig. 5; the dome pressure drop was 4.3%. The measured NO_x reaches a peak of about 3.6 g/kg at a dome equivalence ratio of 0.82. As the dome equivalence ratio exceeds unity, NO_x emission index falls as a result of unburned fuel leaving the combustor.

To place the dome NO_x into context with respect to fuel/air mixing and the type of flame resulting, also shown on Fig. 6 are calculated NO_x curves using two approaches: first, assuming "experimentally perfect premixing" of fuel and air, and second, representing the dome flowfield as a reactor network having a degree of partial stirring. For the experimentally perfect premixing case the empirical correlation of Roffe and Venkataramani[8] for lean premixed propane and air systems was used. In this correlation the residence times were estimated for volumes based on observed flame dimensions. The very simple reactor network for the second examination was based on CFD calculations for this injector and hole pattern, with reactor dimensions based on observed flame dimensions and having the fuel heating value reduced to account for estimated heat losses from the combustor. The network consisted of a perfectly stirred reactor with a parallel plug-flow reactor that processed 13% of the total flow that was recirculated back into the perfectly stirred reactor. These two calculations represent perfect premixing in the dome and well mixed but not perfect premixing. The effect of improved mixing as represented by the two calculations is to increase the peak NO_x and to narrow the NO_x curve across equivalence ratio; furthermore, the peak NO_x occurs at dome equivalence ratios around unity.

Comparing the measured dome NO_x against the two calculations demonstrates that the fuel was actually burned in the dome in far from premixed form. The broadened burning limits and the shift of the NO_x down to about 0.8 equivalence ratio indicates this. This behavior occurs despite the use of a gaseous fuel, intimate association of fuel and air in the fuel injector, and the existence of a flame that is lifted from the injector. Nonetheless, although the dome is not premixed, the NO_x emission indices do still show a strong dependence on dome equivalence ratio over the entire range covered. This is indicative of partially premixed burning, with a level of fuel/air

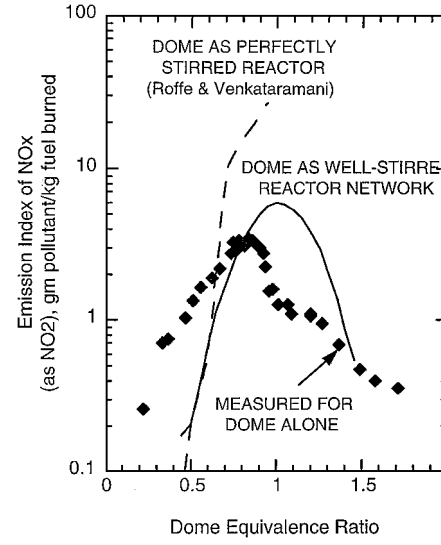

Fig. 6 Assessment of dome mixing characteristics.

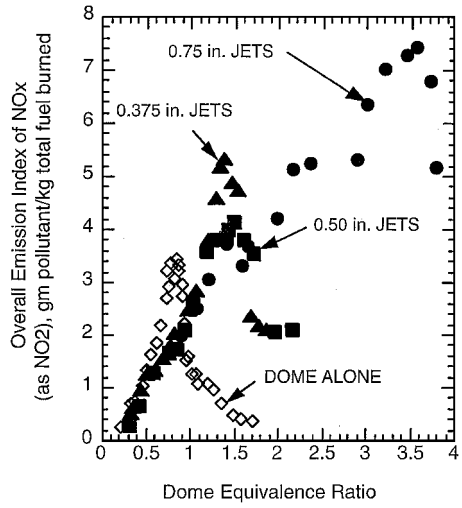

Fig. 7 Overall burning characteristics for NO_x.

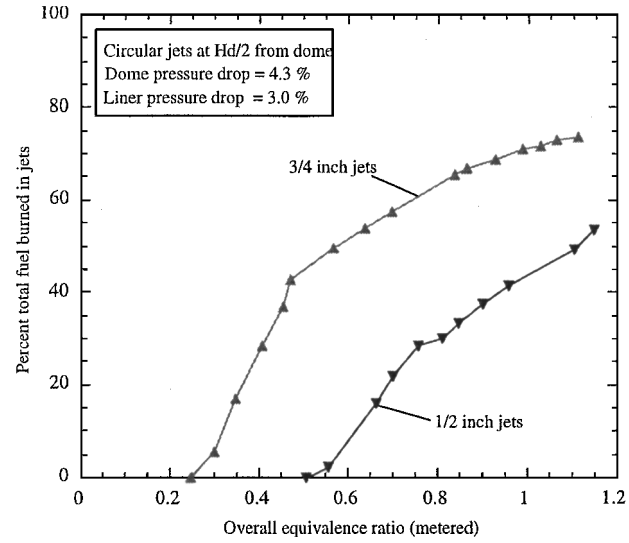

Fig. 8 Dependence of quantity of fuel burned in jets on overall equivalence ratio, for two jet sizes.

unmixedness that is greater than that taken in the reactor network calculations.

Overall Burning Characteristics

If the flame in the dome alone is not premixed, the question must be asked concerning what happens when the air jets are present. Figure 7 is a plot of overall NO_x EIs for several jet systems at $H_d/2$ from the dome, including the dome alone, plotted against dome equivalence ratio, at fixed dome and jet pressure drops. The characteristic of the dome-alone NO_x is that from Fig. 6.

The characteristics for the individual combustion air jets all collapse onto a common curve for dome equivalence ratios up to about 1.15. For dome equivalence ratios of 0.55 and less, this collapsed data is co-incident with the dome-alone data. Such behavior indicates that basic flame characteristics in the dome are unaffected by the presence of the jets.

The NO_x peak for jets being present is shifted from the nominal 0.82 equivalence ratio for the dome-alone to higher dome equivalence ratios, in the range 1.3–1.55 for the smaller jet sizes and to around 3.5 for the largest jet. The levels of NO_x at the peak, and the subsequent behavior on the dome-rich side of the peak, are dependent on the individual jet size. Note, however, that the data for the 0.375-in. (9.53-mm) and 0.50-in. (12.7-mm) jets are virtually co-incident.

The shifted NO_x peak from 0.82 with no jets to 1.3–1.55 dome equivalence ratio with jets indicates that in addition to peak temperatures being reached at lower equivalence ratios (0.82 rather than about 0.92–1.0) as a result of unmixedness effects some of the combustion jet air is actually active in the dome. The co-incidence of the data for individual jets at equivalence ratios less than 1.15 suggests that the dome aerodynamics are not strongly influenced, or least modified, by the details of the air jets, that is, that any additional air introduced into the dome takes part in chemical reactions in a region somewhat separate from the jets themselves and that this region is not far upstream in the dome itself. Flame photographs (Fig. 2) identify a significant luminous region on the injector centerline, just upstream of the confluence of the transverse combustion air jets. This was identified by CFD as burning round a recirculation bubble in this position. This bubble could be where the small quantity of jet air is utilized in the dome. The centerline penetration of all jets at 3% liner pressure drop ensures that this bubble is present whenever the jets are present, although its dimensions depend on the jet size.

Data Analysis Strategy

As Fig. 2 indicates, there are several regions of large heat release existing within the primary zone overall flame structure. To evolve low emissions configurations, it is desirable to understand the separate contributions to overall pollutant formation by these separate burning regions.

A broad bookkeeping strategy was therefore adopted for the data analysis as follows: Because combustion efficiency was 99.99+%, a fuel-rich dome is assumed to burn with 100% oxygen-consumption efficiency at all conditions so that the propane burned in the dome is given by

$$(\dot{m}_{f,\text{dome}})_{\text{burned}} = 0.0638\dot{m}_{a,\text{dome}} \tag{4}$$

and the fuel burned in the jets is

$$(\dot{m}_{f,\text{jets}})_{\text{burned}} = \dot{m}_{f,\text{Tot.}} - (\dot{m}_{f,\text{dome}})_{\text{burned}} \tag{5}$$

Figure 8 shows an example, using the bookkeeping system, of the nominal percent fuel burned in the jets as functions of overall (metered) equivalence ratio for single pairs of opposed circular jets of 0.5 in. (12.7 mm) and 0.75 in. (19.05 mm) diam. The figure shows that for both transverse jets systems the amount of fuel burned in the jets increases with increasing overall equivalence ratio. The 0.75-in. (19.05-mm) jet system at given overall equivalence ratio burns much more of the total fuel supplied than does the 0.50-in. (12.7-mm) jet system. For the 0.75-in. (19.05-mm) jet system all of the fuel supplied is burned in the dome for overall equivalence ratios less than 0.25; for the 0.50-in. (12.7-mm) jet system all of the supplied fuel is burned in the dome for overall equivalence ratios less than 0.5.

Figure 9 shows the burning zone equivalence ratio variations with overall (metered) equivalence ratio for dome and jets at each hole configuration. The relationships between overall and dome and jet equivalence ratios are, respectively, given by

$$\phi_{\text{dome}} = \left(1 + \frac{\dot{m}_{a,\text{jets}}}{\dot{m}_{a,\text{dome}}}\right)\phi_{\text{overall}} \tag{6}$$

and

$$\phi_{\text{jets}} = \frac{\dot{m}_{f,\text{jets}}}{0.0638\dot{m}_{a,\text{jets}}} \tag{7}$$

It can be seen from Fig. 9 that at any overall equivalence ratio the dome with the 0.75-in. (19.05-mm) liner jets is much richer than the dome with 0.5-in. (12.7-mm) jets. For the 0.75-in. (19.05-mm) jets the dome is always above stoichiometric in the range of overall equivalence ratios covered; for the 0.5-in. (12.7-mm) jets the dome is either fuel lean or fuel rich, depending on the overall equivalence ratio. For overall equivalence ratios up to unity, the jets are always fuel lean for either jet size. As a consequence of the stoichiometry distributions for the two jet sizes, the 0.75-in. (19.05-mm) jets burn much more of the total fuel than do the 0.50-in. (12.7-mm) jets.

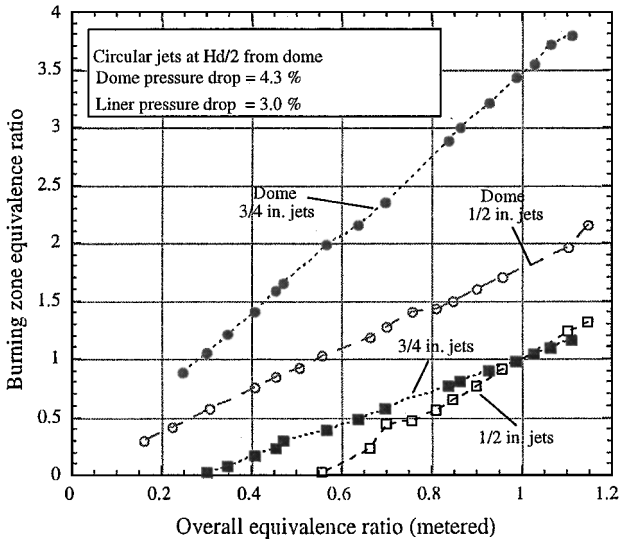

Fig. 9 Stoichiometry breakdowns between dome and jets, for two jet sizes.

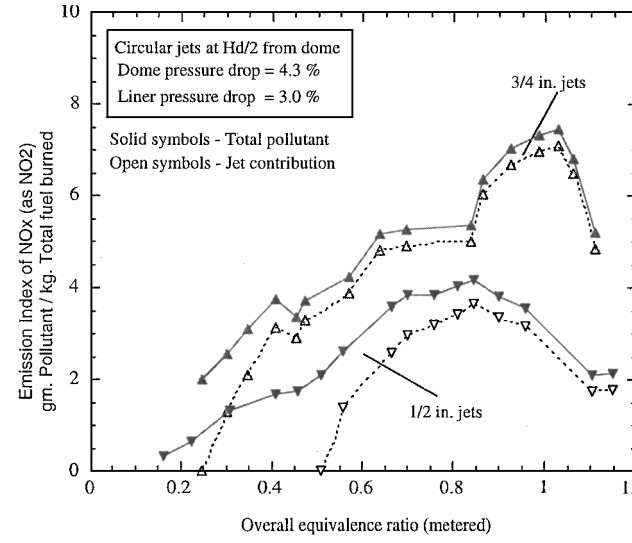

Fig. 10 Contributions of jet NO_x to overall NO_x for two jet systems.

Jet Contribution to NO_x Generation

The principal of superpositions can be used to obtain the separate contributions to total NO_x of the dome alone and then the air jet system. Superpositions depend on the two elements being considered as not substantially changing each other. This has been shown for NO_x in Fig. 7. Therefore, the jet-NO_x EIs were obtained by subtracting from the total NO_x EIs the NO_x EIs for the dome. The dome EIs were obtained from the dome-alone curve in Fig. 6 at the appropriate dome equivalence ratios for each jet system with a particular overall equivalence ratio.

In Fig. 10 the EIs of NO_x, in terms of grams of NO_x per kilogram of total fuel burned, for the 0.50-in. (12.7-mm) and 0.75-in. (19.05-mm) initial diameter transverse combustion air jets are presented with variation in overall (metered) equivalence ratio. For each jet size the total NO_x and the NO_x generated by just the transverse jet systems are given. The figure shows that the jet NO_x reaches zero for the 0.75-in. (19.05-mm) jets at an overall equivalence ratio of 0.25 and for the 0.5-in. (12.7-mm) jets at an overall equivalence ratio of 0.51. These values correspond to zero jet equivalence ratios and zero fuel burned in the jets, as shown in Figs. 8 and 9. These agreements support the use of superpositions as a means to extract jet NO_x. At lower overall equivalence ratios all of the NO_x for both jet systems is generated in the dome, even though the jets are present. For overall equivalence ratios of less than about 0.25, the two overall NO_x curves should run into each other for a common curve representing dome-only (Fig. 6) burning. Although the two curves are converging at lower equivalence ratios, they are not co-incident for overall equivalence ratios less than 0.25. This is because there are slightly different aerodynamic blockage effects resulting from the two transverse jet systems and acting upon the axially directed fuel/air jet from the injector/dome interface region.

The strong jet-NO_x effect is illustrated in Fig. 11, which plots for each jet system the jet NO_x EIs, expressed as grams of NO_x per kilogram of fuel burned in the jets, against the jet equivalence ratio. Expressed in this form, the fact that the 0.75-in. (19.05-mm) jet system burns considerably more of the total fuel supplied than does the 0.50-in. (12.7-mm) jet system (Fig. 8) should be accounted for. Data are shown for all of the jet diameters evaluated. For jet equivalence ratios less than 0.8–0.9 (where a NO_x peak is expected for partially premixed systems) the NO_x for the 0.375-in. (9.53-mm), 0.50-in. (12.7-mm), and 0.75-in. (19.05-mm) jets is essentially independent of jet equivalence ratio. This suggests that the fuel burned in these jet systems at such lower equivalence ratios is in reality reacted in stoichiometric interfaces associated with the fresh air entering through the jets. The jet NO_x EIs consistently begin to decrease at higher jet equivalence ratios. This is because unburned fuel is now exiting the

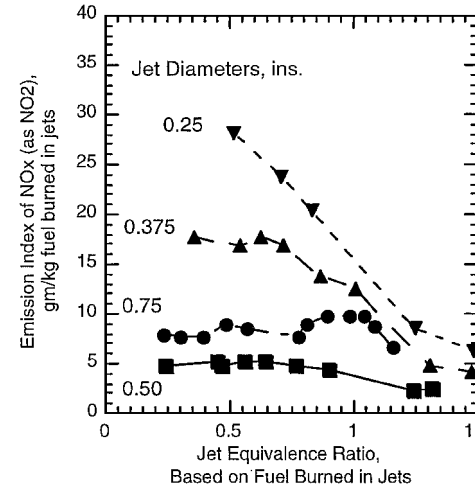

Fig. 11 Demonstration of stoichiometric burning in jet systems.

combustor because the available stoichiometric surfaces are burning all the fuel that they can. The jet NO_x EI plateau levels for the lower jet equivalence ratios decrease with increasing jet initial diameter, with the exception of the 0.50-in. (12.7-mm) jet system, which unexpectedly has the lowest values. For the 0.25-in. (6.35-mm) jets the jet NO_x EIs continuously decrease with increasing jet equivalence ratio over the entire range covered. This suggests that because of its small initial size this jet system might be less coherent than the other jet systems. Although the jet systems are conveniently identified by the jet initial diameters, the flame structures associated with each also include that of the central "football" recirculation zone. For given operating conditions the sizes of these recirculation zones depend on the jet dimensions.

The percentage of total NO_x that is generated in the jets for each initial jet size is plotted in terms of overall equivalence ratio in Fig. 12. The percent jet NO_x was obtained by multiplying the calculated emission indices for the jets by the mass flow rate of fuel burned in the jets, divided by the measured overall emission index for the complete primary zone at the same equivalence ratio, multiplied by the total fuel flow rate. The figure shows that for the 0.75-in. (19.05-mm) initial jet size more than half of the NO_x originates in the jets for all operating equivalence ratios; for the 0.50-in. (12.7-mm) jet the jet NO_x only reaches 50% of the total for a stoichiometric primary zone. The general behavior is for the percent jet NO_x to increase with overall equivalence ratio and to do so rather steeply initially until a plateau level is reached. This behavior is repeated

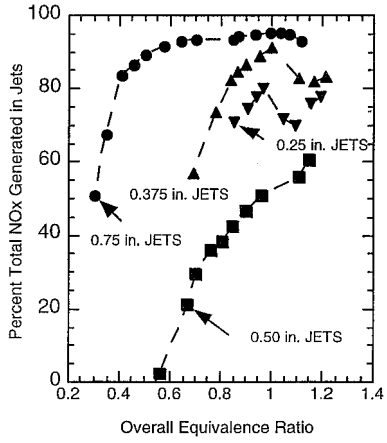

Fig. 12 Contribution of jet-generated NO_x.

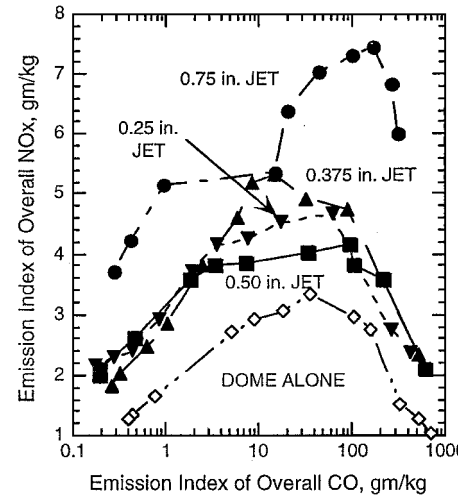

Fig. 13 Overall emissions assessment for range of jet sizes.

for each jet system, and the plateau level is lower for smaller jets than for the larger jets. For the 0.75-in. (19.05-mm) jets the plateau is at about 95% jet NO_x; for the 0.375-in. (9.53-mm) jets it is about 85%, and for the 0.25-in. (6.35-mm) jets it is about 75%. The 0.5-in. (12.70-mm) jet system has not yet reached its plateau level in the range of overall equivalence ratios covered. This jet system appears to be the exception to the general behavior. If overall equivalence ratio is increased above unity, the percent jet NO_x contribution to overall NO_x would eventually start to fall as the jet system became overrich and unburned fuel left the primary zone. This behavior is clearly evident for the two smaller jets and is becoming so for the largest jet. The 50% jet NO_x condition is reached at overall equivalence ratios that increase with decreasing jet size. This corresponds to the condition where the dome equivalence ratio exceeds unity in each case. For the 0.50-in. (12.70-mm) jet system the 50% jet NO_x condition is reached at an overall equivalence ratio of 0.96. From stoichiometry plots (Fig. 9) this corresponds to a dome equivalence ratio of 1.7. This is a very rich dome condition compared to the other jet sizes. This jet system generates lower jet NO_x percentages at all overall equivalence ratios than either larger or smaller jets. Clearly, the 0.5-in. (12.70-mm) jet system behaves differently to all of the others. This different behavior appears to be associated with the football recirculation zone. For the 0.375-in. (9.53-mm) and 0.25-in. (6.35-mm) air jets the recirculation zones are observed to be physically very small. For the 0.75-in. (19.05-mm) air jets although the recirculation zone is physically larger, it is small in relation to the jet structures themselves. In the case of the 0.50-in. jets, the recirculation and jet structures are observed to be comparable in size. The relative dimensions of the recirculation bubble and jet envelope flames can be appreciated from Fig. 2. A clear implication of Fig. 12 in light of these observations concerning the football recirculation bubble is that unburned fuel from the dome is burned differently in the recirculation bubble than it is around the jet structures. It is not difficult to accept that combustion around the highly coherent air jet structures takes place stoichiometrically. This being so, the hypothesis leads to the conclusion that combustion in the recirculation bubble must therefore take place partially premixed and at a local equivalence ratio less than unity. The jet-system net NO_x generated therefore would represent a combination of the NO_x from these two sources, and the amount of NO_x would depend on how much of the fuel is burned around the jets and how much is burned in the recirculation region. If a significant portion of the total fuel processed by the 0.50-in. (12.7-mm) jet system is reacted partially premixed in the recirculation bubble, then the NO_x of this system would be lower than anticipated from just the jet diameter.

Overall Emissions Assessment

Figure 13 is a plot of overall NO_x emissions indices against overall CO emissions indices for each of the jet sizes, including the dome alone. The data for each jet size are limited on the left-hand side by a 0.5 primary zone equivalence ratio and on the right-hand side by 1.1 primary zone equivalence ratio. Such a plot represents the emissions trade between NO_x and CO that might be made. A box can be placed around the data for any particular jet size in the plot, bounded on one side by the maximum CO, on the top by maximum NO_x, and on the remaining side and the bottom by the respective axes. Such a box is a qualitative measure of the total emissions production of the particular jet configuration. Data for any other configuration over the same equivalence ratio range that fall wholly inside the initial box represent a truly lower emissions configuration.

Review of the figure reveals several interesting facts. First, the dome-alone configuration does truly represent the lowest emissions configuration because it has the smallest box. Second, the 0.50-in. (12.70-mm) jet does indeed represent some kind of optimum jet configuration for this primary zone because its box is smaller than the boxes for the other jets. It does not achieve its low NO_x by producing large amounts of CO. Third, the 0.75-in. (19.05-mm) jet is the worst emissions producer, and this is through its jet NO_x generation. The levels of CO over the equivalence ratio range in Fig. 13 are all at or very close to the appropriate equilibrium levels for the test conditions. For lower equivalence levels outside the range, there is an upward departure from equilibrium CO as a LBO condition is approached; similarly, at higher equivalence ratios there is also an upward departure from equilibrium CO as a result of a lack of oxygen.

LBO Considerations

The finding that the dome-alone configuration, that is, no traverse air jets whatsoever, gives the lowest emissions and raises the valid question as to the need for the separate combustion air jets.

The combustion air jets are needed to reduce flame length and to enhance lean stability. These are especially important for aircraft applications. Figure 14 shows some limited stability data for the dome alone and for the dome with the 0.50-in. (12.70-mm) jets at the $H_d/2$ position, in the form of blowout overall equivalence ratio against the air loading parameter (ALP)[9]. The ALP is defined as

$$ALP = m/(VP^n F) \tag{8}$$

The blowouts were conducted at atmospheric pressure, with variation of dome pressure drop for the dome alone and liner pressure drop at fixed dome pressure drop for the with-jet case. In addition for the dome-alone case, two inlet air temperatures were used—ambient and 500°F (533 K). The plot shows that for given ALP the with-jets case blows out at lower equivalence ratio than does the dome alone. For the dome-alone situation there were several flame modes observed. Blowouts for the range of ALPs in Fig. 14 were governed by lifted and attached flame conditions.[2] The presence of the combustion air jets exerts a backpressure on the flame and in addition provides for flame holding on the jets when the flame is lifted from the injector.

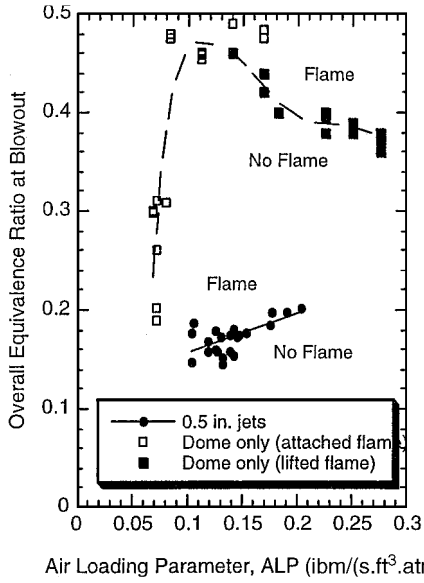

Fig. 14 Stability plot for dome alone and dome with 0.50-in. (12.7-mm) jets at half-dome height position.

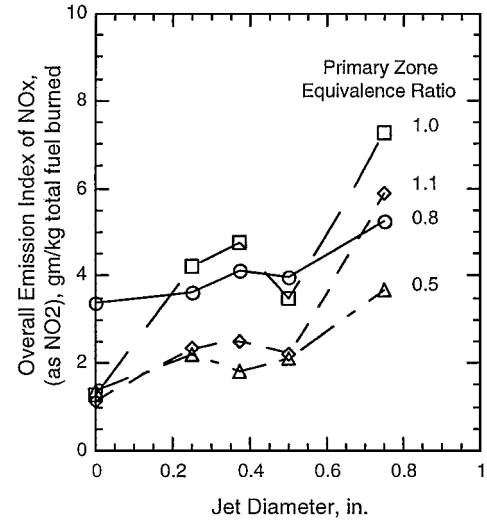

Fig. 15 Optimum jet size for minimum NO_x from overall primary zone.

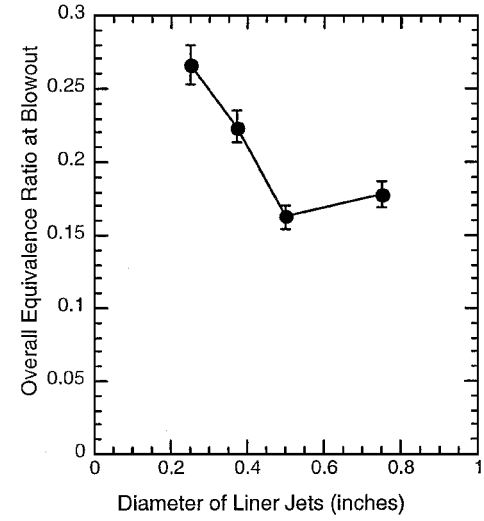

Fig. 16 Optimum jets diameter for blowout stability.

Discussion

The study reveals that the use of transverse combustion air jets to terminate and close the conventional primary zone of an aircraft gas-turbine combustor results in a severe penalty in NO_x emissions as a result of the formation of stoichiometric fuel/air burning interfaces around the jets. Most of the NO_x formed originates in these interfaces. The lowest overall emission characteristic would be achieved from a dome-alone primary zone. However, without the presence of combustion air jets the dome-alone blowout stability is inadequate for the wide turndown ratio necessary for the multipoint operating requirement for aircraft applications. Truly low NO_x dome-alone configurations would demand improved fuel/air mixing compared to conventional primary zones and selection of a fuel-lean design point, together with staged combustion in order to achieve adequate blowout stability. When a conventional dome design is used and the design requirements also include blowout stability as well as low emissions, combustion air jets must be used.

It does appear possible to achieve adequate blowout stability, together with minimized NO_x emissions, by optimizing the combustion air jet system. An example of low NO_x/adequate blowout margin optimization is shown in Figs. 15 and 16. Figure 15 gives the overall emission index of NO_x in terms of primary zone equivalence ratio at a high-power design point for an opposed pair of jets situated in line with the fuel injector at one-half a dome height downstream from the dome. Dome and liner pressure drops are fixed and are in line with current design practice. For a fixed geometry combustor, a primary zone design point equivalence ratio of 1.1 gives a value at engine idle power that will result in low CO emissions. Figure 16 shows that best lean blowout performance would be achieved with 0.50-in.-(12.7-mm) diam circular jets. It can be seen from Fig. 15 that the 0.50-in. (12.7-mm) jets would give a NO_x performance that is equivalent to operating the primary zone very lean (0.5 equivalence ratio) at design point. It should be understood that selection of a 1.1 primary zone equivalence ratio would necessitate the provision of additional combustion air downstream of the primary zone. Again, optimization of this jet system is then necessary.

The optimization involves a minimization of the stoichiometric interfaces formed around the air jets, together with achieving some partial premixing of jet air with unburned combustion products delivered from the dome. This apparently involves careful matching of the jet system to the fuel/air distributions delivered to the air jets by the dome. In the design process a heavy reliance on the computational fluid dynamics tool is essential to achieve the flame structures desired. Experimentally, assessments of local equivalence ratios in the primary zone would be demanded to evaluate these structures. Fortunately, one- and two-color optical diagnostic tools relying on chemiluminescence are now becoming available for this purpose.

A key feature of the optimization appears to be the formation of the football recirculation zones formed on the upstream side of the colliding opposed air jets. The term recirculation zone generally implies a closed volume of fluid, within which little chemical reaction takes place as a result of poor interchange with the surroundings. However, dynamic behavior, wherein the recirculation zone collapses and then reforms at a relatively high frequency, is generally considered to be the mechanism for combustion in such zones. Whereas dynamic behavior is almost certainly of some importance here, it should be accepted the term "recirculation zone" is not a very good descriptor of the "footballs." These are actually highly three-dimensional structures that wrap around the air jets in complicated fashion. They are not closed bodies, but receive fresh air from the colliding jets that give rise to them and discharge products into the wakes of the jets that they wrap around; flow from the dome in engulfed as the footballs roll up.

The study indicates that combustor design requirements, such as blowout stability and emissions, cannot be pursued independently. They must be worked together.

Conclusions

1) Most of the NO_x generated in the generic primary zone appears to originate from stoichiometric burning in interfaces around the combustion air jet system.

2) Minimum total emissions are produced when all of the reactants are introduced through the combustor dome.

3) Combustion air jets are necessary to reduce flame length and confer lean blowout stability.

4) For reasons associated with minimizing the stoichiometric interfaces around the jet and the amount of fuel that is burned in them, the 0.50-in.-(12.70-mm) diam opposed circular jets exhibit a clear optimum for the primary zone when the jets are positioned half a dome height downstream. This optimum is for minimum NO_x and lean blowout stability.

Acknowledgments

The enthusiasm, motivation, support, and contributions of W. M. Roquemore are greatly appreciated. The authors wish to thank R. Britton, M. Burns, and M. Russell for their help in acquiring emission measurements. This research was sponsored by the U.S. Air Force Wright Laboratory, Aero Propulsion and Power Directorate, under Contract F33615-93-C-2304 to Pratt & Whitney, East Hartford, Connecticut (Contract Monitor: Dale Shouse).

References

[1]Sturgess, G. J., Sloan, D. G., Roquemore, W. M., Reddy, V. K., Shouse, D., Lesmerises, A. L., Ballal, D. R., Heneghan, S. P., Vangsness, M. D., and Hedman, P. O., "Flame Stability and Lean Blowout—A Research Program Progress Report," *Proceedings of the 10th International Symposium on Air Breathing Engines*, edited by F. S. Billig, Vol. 1, International Symposium on Air Breathing Engines, Nottingham, England, 1991, pp. 372–384.

[2]Hedman, P. O., Sturgess, G. J., Warren, D. L., Goss, L. P., and Shouse, D. T., "Observations of Flame Behavior from a Practical Fuel Injector Using Gaseous Fuel in a Technology Combustor," *Journal of Engineering for Gas Turbines and Power*, Vol. 117, No. 3, 1995, pp. 441–452.

[3]Sturgess, G. J., Heneghan, S. P., Vangsness, M. D., Ballal, D. R., Lesmerises, A. L., and Shouse, D., "Effects of Back Pressure in a Lean Blowout Research Combustor," *Journal of Engineering for Gas Turbines and Power*, Vol. 115, No. 3, 1993, pp. 486–498.

[4]Spalding, D. B., "Performance Criteria of Gas-Turbine Combustion Chambers—A Method of Comparison and Selection for the Designer," *Aircraft Engineering Monograph*, Bunhill Publications Ltd., London, 1956.

[5]Gerrard, A. J., "Methods of Flow Visualization By Means of Water," *Experimental Methods in Combustion Research*, edited by J. Surugue, Pergamon, New York, 1961, Sec. 1-10, pp. 22–43.

[6]Sturgess, G. J., McKinney, R. G., and Morford, S. A., "Modification of Combustor Stoichiometry for Reduced NO_x Emissions from Aircraft Engines," *Journal of Engineering for Gas Turbines and Power*, Vol. 115, No. 3, 1993, pp. 570–580.

[7]Sturgess, G. J., and Shouse, D. T., "A Hybrid Model for Calculating Lean Blowouts in Practical Combustors," AIAA Paper-96-3125, July 1996.

[8]Roffe, G., and Venkataramani, K. S., "Emissions Measurements for Lean Premixed Propane/Air Systems at Pressure up to 30 Atmospheres," NASA Rept. CR-159421, 1978.

[9]Sturgess, G. J., and Shouse, D., "Lean Blowout in a Generic Gas Turbine Combustor with High Optical Access," *Journal of Engineering for Gas Turbines and Power,* Vol. 119, No. 1, 1997, pp. 108–118.